MIT Open Access Articles

Angular analysis of charged and neutral B → Kμ[superscript +]μ[superscript −] decays

Angular analysis of charged and neutral $B \to K\mu^+\mu^-$ decays

The LHCb collaboration

E-mail: p.owen10@imperial.ac.uk

ABSTRACT: The angular distributions of the rare decays $B^+ \to K^+\mu^+\mu^-$ and $B^0 \to K^0_S\mu^+\mu^-$ are studied with data corresponding to $3\,\text{fb}^{-1}$ of integrated luminosity, collected in proton-proton collisions at 7 and $8\,\text{TeV}$ centre-of-mass energies with the LHCb detector. The angular distribution is described by two parameters, F_H and the forward-backward asymmetry of the dimuon system A_FB, which are determined in bins of the dimuon mass squared. The parameter F_H is a measure of the contribution from (pseudo)scalar and tensor amplitudes to the decay width. The measurements of A_FB and F_H reported here are the most precise to date and are compatible with predictions from the Standard Model.

Contents

1 Introduction

The $B^+ \to K^+\mu^+\mu^-$ and $B^0 \to K^0_S\mu^+\mu^-$ decays are rare, flavour-changing neutral-current processes that are mediated by electroweak box and penguin amplitudes in the Standard Model (SM).[1] In well motivated extensions of the SM [1, 2], new particles can introduce additional amplitudes that modify the angular distribution of the final-state particles predicted by the SM.

In this paper, the angular distributions of the final-state particles are probed by determining the differential rate of the B meson decays as a function of the angle between the direction of one of the muons and the direction of the K^+ or K^0_S meson in the rest frame of the dimuon system. The analysis is performed in bins of q^2, the dimuon invariant mass squared. The angular distribution of $B^+ \to K^+\mu^+\mu^-$ decays has previously been studied by the BaBar [3], Belle [4], CDF [5] and LHCb [6] experiments with less data.

For the decay $B^+ \to K^+\mu^+\mu^-$, the differential decay rate can be written as [2, 7]

$$\frac{1}{\Gamma}\frac{d\Gamma}{d\cos\theta_l} = \frac{3}{4}(1 - F_{\rm H})(1 - \cos^2\theta_l) + \frac{1}{2}F_{\rm H} + A_{\rm FB}\cos\theta_l \,, \tag{1.1}$$

where θ_l is the angle between the direction of the μ^- (μ^+) lepton and the K^+ (K^-) meson for the B^+ (B^-) decay. The differential decay rate depends on two parameters, the forward-backward asymmetry of the dimuon system, $A_{\rm FB}$, and a second parameter $F_{\rm H}$,

---

[1]The inclusion of charge conjugated processes is implied throughout.

which corresponds to the fractional contribution of (pseudo)scalar and tensor amplitudes to the decay width in the approximation that muons are massless. The decay width, A_{FB} and F_{H} all depend on q^2.

The structure of eq. (1.1) follows from angular momentum conservation in the decay of a pseudo-scalar B meson into a pseudo-scalar K meson and a pair of muons. In contrast to the decay $B^0 \to K^{*0}\mu^+\mu^-$, A_{FB} is zero up to tiny corrections in the SM. A sizable value of A_{FB} is possible in models that introduce large (pseudo)scalar- or tensor-like couplings [1, 2]. The parameter F_{H} is non-zero, but small, in the SM due to the finite muon mass. For eq. (1.1) to remain positive at all lepton angles, A_{FB} and F_{H} have to satisfy the constraints $0 \le F_{\mathrm{H}} \le 3$ and $|A_{\mathrm{FB}}| \le F_{\mathrm{H}}/2$.

Since the B^0 and $\overline{B}^0$ meson can decay to the same $K^0_{\mathrm{s}}\mu^+\mu^-$ final state, it is not possible to determine the flavour of the B meson from the decay products. Without tagging the flavour of the neutral B meson at production, it is therefore not possible to unambiguously chose the correct muon to determine θ_l. For this reason, θ_l is always defined with respect to the μ^+ for decays to the $K^0_{\mathrm{s}}\mu^+\mu^-$ final-state. In this situation any visible A_{FB} would indicate that there is either a difference in the number of B^0 and $\overline{B}^0$ mesons produced, CP violation in the decay or that the A_{FB} of the B^0 and $\overline{B}^0$ decay differ. Any residual asymmetry can be canceled by performing the analysis in terms of $|\cos\theta_l|$,

$$\frac{1}{\Gamma}\frac{\mathrm{d}\Gamma}{\mathrm{d}|\cos\theta_l|} = \frac{3}{2}(1 - F_{\mathrm{H}})(1 - |\cos\theta_l|^2) + F_{\mathrm{H}}\,, \tag{1.2}$$

where the constraint $0 \le F_{\mathrm{H}} < 3$ is needed for this expression to remain positive at all values of $|\cos\theta_l|$. This simplification of the angular distribution is used for the $B^0 \to K^0_{\mathrm{s}}\mu^+\mu^-$ decay in this paper.

2 Data and detector description

The data used for the analysis correspond to $1\,\mathrm{fb}^{-1}$ of integrated luminosity collected by the LHCb experiment in pp collisions at $\sqrt{s} = 7\,\mathrm{TeV}$ in 2011 and $2\,\mathrm{fb}^{-1}$ of integrated luminosity collected at $\sqrt{s} = 8\,\mathrm{TeV}$ in 2012. The average number of pp interactions, yielding a charged particle in the detector acceptance, per bunch crossing was 1.4 in 2011 and 1.7 in 2012.

The LHCb detector [8] is a single-arm forward spectrometer covering the pseudorapidity range $2 < \eta < 5$, designed for the study of particles containing b or c quarks. The detector includes a high-precision tracking system consisting of a silicon-strip vertex detector surrounding the pp interaction region, a large-area silicon-strip detector located upstream of a dipole magnet with a bending power of about $4\,\mathrm{Tm}$, and three stations of silicon-strip detectors and straw drift tubes [9] placed downstream of the magnet. The combined tracking system provides a momentum measurement with relative uncertainty that varies from 0.4% at $5\,\mathrm{GeV}/c$ to 0.6% at $100\,\mathrm{GeV}/c$, and impact parameter resolution of $20\,\mu\mathrm{m}$ for tracks with large transverse momentum. Different types of charged hadrons are distinguished by information from two ring-imaging Cherenkov detectors [10]. Photon, electron and hadron candidates are identified by a calorimeter system consisting of scintillating-pad and preshower detectors, an electromagnetic calorimeter and a hadronic

calorimeter. Muons are identified by a system composed of alternating layers of iron and multiwire proportional chambers [11].

Samples of simulated $B^+ \to K^+\mu^+\mu^-$ and $B^0 \to K_S^0\mu^+\mu^-$ decays are used to understand how the detector geometry, the reconstruction and subsequent event selection bias the angular distribution of the decays. In the simulation, pp collisions are generated using PYTHIA [12] with a specific LHCb configuration [13]. Decays of hadronic particles are described by EVTGEN [14], in which final state radiation is generated using PHOTOS [15]. The interaction of the generated particles with the detector and its response are implemented using the GEANT4 toolkit [16, 17] as described in ref. [18].

3 Selection of signal candidates

The LHCb trigger system [19] consists of a hardware stage, based on information from the calorimeter and muon systems, followed by a software stage, which applies a full event reconstruction. In the hardware stage of the trigger, candidates are selected with at least one muon candidate with transverse momentum, $p_T > 1.48\,(1.76)\,\mathrm{GeV}/c$ in 2011 (2012). In the second stage of the trigger, at least one of the final-state particles from the B^0 or B^+ meson decay is required to have $p_T > 1.0\,\mathrm{GeV}/c$ and impact parameter larger than $100\,\mu\mathrm{m}$ with respect to any primary vertex (PV) from the pp interactions in the event. Tracks from two or more of the final-state particles are required to form a secondary vertex that is displaced from all of the PVs.

The K_S^0 mesons from the decay $B^0 \to K_S^0\mu^+\mu^-$ are reconstructed through their decay $K_S^0 \to \pi^+\pi^-$ in two different categories: the first category contains K_S^0 mesons that decay early enough that the final-state pions are reconstructed in the vertex detector; and the second contains K_S^0 mesons that decay later, such that the first track segment that can be reconstructed is in the large-area silicon-strip detector. These categories are referred to as *long* and *downstream*, respectively. Candidates in the long category have better mass, momentum and vertex resolution.

Reconstructed tracks that leave hits in the LHCb muon system are positively identified as muons. Two muons of opposite charge are then combined with either a track (K^+) or a reconstructed K_S^0 to form a B^+ or B^0 candidate. The $\pi^+\pi^-$ pair from the reconstructed K_S^0 is constrained to the known K_S^0 mass when determining the mass of the B^0 candidate. Neural networks, using information from the RICH detectors, calorimeters and muon system, are used to reject backgrounds where either a pion is misidentified as the kaon in the B^+ decay or a pion or kaon are incorrectly identified as one of the muons.

An initial selection is applied to B^+ and B^0 candidates to reduce the level of the background. The selection criteria are common to those described in ref. [20]: the $\mu^\pm$ and the K^+ candidates are required to have $\chi^2_{\mathrm{IP}} > 9$, where χ^2_{IP} is defined as the minimum change in χ^2 of the vertex fit to any of the PVs in the event when the particle is added to that PV; the dimuon pair vertex fit has $\chi^2 < 9$; the B candidate is required to have a vertex fit $\chi^2 < 8$ per degree of freedom; the B momentum vector is aligned with respect to one of the PVs in the event within $14\,\mathrm{mrad}$, the B candidate has $\chi^2_{\mathrm{IP}} < 9$ with respect to that PV and the vertex fit χ^2 of that PV increases by more than 121 when including the B decay products. In addition, the K_S^0 candidate is required to have a decay time larger than $2\,\mathrm{ps}$.

The initial selections are followed by tighter multivariate selections, based on boosted decision trees (BDTs) [21] with the AdaBoost algorithm [22]. The working points for the BDTs are chosen to maximise $N_{\mathrm{S}}/\sqrt{N_{\mathrm{S}} + N_{\mathrm{B}}}$, where N_{S} and N_{B} are the expected numbers of signal and background candidates within $\pm 50 \, \mathrm{MeV}/c^2$ of the known B^0 or B^+ meson masses, respectively. For the $B^+ \to K^+ \mu^+ \mu^-$ decay, the variables used in the BDT are identical to those of ref. [20]. In contrast to that analysis, however, the multivariate selection is trained using a sample of simulated events to model the signal and candidates from the data with $K^+ \mu^+ \mu^-$ invariant masses in the range $5700 < m(K^+ \mu^+ \mu^-) < 6000 \, \mathrm{MeV}/c^2$ for the background. This background sample is not used in the subsequent analysis, where the invariant mass of the candidates is restricted to the range $5170 < m(K^+ \mu^+ \mu^-) < 5700 \, \mathrm{MeV}/c^2$. The multivariate selection has an efficiency of 89% for signal and removes 94% of the background that remains after the initial selection. For the $B^0 \to K_{\mathrm{S}}^0 \mu^+ \mu^-$ decay, two independent BDTs are trained for the long and downstream categories. Samples of simulated events are used in the signal training and candidates from the data with masses $5700 < m(K_{\mathrm{S}}^0 \mu^+ \mu^-) < 6000 \, \mathrm{MeV}/c^2$ for the background training. The following information is used in the classifiers: the B^0 candidate momentum and p_{T}, its vertex quality (χ^2) and decay time, the K_{S}^0 candidate p_{T}, and the angle between the B^0 candidate momentum and the direction between the PV and the B^0 decay vertex. For the long category, the K_{S}^0 candidate χ_{IP}^2 is also included. The multivariate selection removes 99% of the combinatorial background and is 66% and 48% efficient for the long and downstream signal categories.

Combinatorial backgrounds for the $B^+ \to K^+ \mu^+ \mu^-$ decay, where the K^+, μ^+ and μ^- candidates do not all come from the same b-hadron decay, are reduced to a small level by the multivariate selection. After applying the multivariate selection, the signal-to-background ratio in a $\pm 50 \, \mathrm{MeV}/c^2$ range around the known B^+ mass is better than six-to-one. Remaining backgrounds mainly come from b-hadron decays that are fully or partially reconstructed in the detector. The $B^+ \to J/\psi K^+$ and $B^+ \to \psi(2S) K^+$ decays[2] are rejected by removing the regions of dimuon mass around the charmonium resonances ($8.0 < q^2 < 11.0 \, \mathrm{GeV}^2/c^4$ and $12.5 < q^2 < 15.0 \, \mathrm{GeV}^2/c^4$). These decays can also form a background to the $B^+ \to K^+ \mu^+ \mu^-$ decay if the kaon is incorrectly identified as a muon and the muon with the same charge is incorrectly identified as a kaon. This background is removed by rejecting candidates with a $K^+ \mu^-$ pair whose invariant mass (under the $\mu^+ \mu^-$ mass hypothesis) is consistent with that of the J/ψ or $\psi(2S)$ meson, if the reconstructed kaon can also be matched to hits in the muon system. A narrow range in q^2 from $0.98 < q^2 < 1.10 \, \mathrm{GeV}^2/c^4$ is also removed to reject $B^+ \to \phi K^+$ decays, followed by the $\phi \to \mu^+ \mu^-$ decay. The region $m(K^+ \mu^+ \mu^-) < 5170 \, \mathrm{MeV}/c^2$ is contaminated by partially reconstructed b-hadron decays such as $B^0 \to K^{*0} \mu^+ \mu^-$ where the pion from the $K^{*0} \to K^+ \pi^-$ decay is not reconstructed. This region is not used in the subsequent analysis and dictates the lower bound of the $5170 < m(K^+ \mu^+ \mu^-) < 5700 \, \mathrm{MeV}/c^2$ mass range. Backgrounds from fully hadronic b-hadron decays, such as the decay $B^+ \to K^+ \pi^+ \pi^-$, are reduced to a

---

[2]Throughout this paper the decays $B^+ \to J/\psi K^+$ and $B^0 \to J/\psi K_{\mathrm{S}}^0$ refer to decays of B^+ and B^0 mesons to $K^+ \mu^+ \mu^-$ and $K_{\mathrm{S}}^0 \mu^+ \mu^-$ final-states, respectively, through the decay $J/\psi \to \mu^+ \mu^-$.

negligible level using stringent muon-identification selection criteria. A further requirement is applied on the $K^+\mu^-$ pair to remove a small contribution from $B^+ \to \overline{D}^0\pi^+$ decays with $\overline{D}^0 \to K^+\pi^-$, where the pions survive the muon-identification requirements. Candidates are rejected if the mass of the $K^+\mu^-$ pair, computed under the $K^+\pi^-$ hypothesis, is in the range $1850 < m(K^+\pi^-) < 1880\,\mathrm{MeV}/c^2$. After the application of all selection criteria, the background from other b-hadron decays is reduced to $\mathcal{O}(0.1\%)$ of the level of the signal. The total efficiency for reconstructing and selecting the $B^+ \to K^+\mu^+\mu^-$ decay is around 2%.

Due to the long lifetime of the K^0_S meson, there are very few b-hadron decays that can be mistakenly identified as $B^0 \to K^0_S\mu^+\mu^-$ decays. The largest source of fully reconstructed background is the decay $\Lambda^0_b \to \Lambda\mu^+\mu^-$, where the proton from the $\Lambda \to p\pi^-$ decay is incorrectly identified as a π^+. This background is removed by rejecting K^0_S meson candidates if the mass of the $\pi^+\pi^-$ pair, under the $p\pi^-$ mass hypothesis, is consistent with that of a Λ baryon within $\pm10\,\mathrm{MeV}/c^2$ ($\pm15\,\mathrm{MeV}/c^2$) for long (downstream) candidates. This veto is 95% efficient on genuine K^0_S meson decays and removes more than 99% of Λ baryons. The total efficiency for reconstructing the $B^0 \to K^0_S\mu^+\mu^-$ decay is about 0.2%, which is a factor of ten lower than for the charged decay. This is due to a combination of three effects: the long flight distance of K^0_S mesons in the detector, the $K^0_S \to \pi^+\pi^-$ branching fraction, and the requirement of having four, rather than three, tracks within the detector acceptance. After applying the selection procedure, the signal-to-background ratio in a $\pm50\,\mathrm{MeV}/c^2$ range around the known B^0 mass is better than three-to-one for the $B^0 \to K^0_S\mu^+\mu^-$ decay.

After applying the full selection criteria, more than 99% of the selected events contain only one B^+ or B^0 candidate. Events containing more than one candidate have all but one candidate removed at random in the subsequent analysis.

4 Angular acceptance

The geometrical acceptance of the LHCb detector, the trigger and the event selection can all bias the $\cos\theta_l$ distribution of the selected candidates. The angular acceptance is determined using a sample of simulated signal events. The acceptance as a function of $\cos\theta_l$ is parameterised using a fourth-order polynomial function, fixing the odd-order terms to zero so that the acceptance is symmetric around zero. Any small asymmetry in the acceptance for B and $\overline{B}$ mesons, due to charge asymmetries in the reconstruction, cancels when combining B and $\overline{B}$ meson decays.

At small values of q^2, there is a large reduction of the signal efficiency at values of $\cos\theta_l$ close to ±1, as seen in figure 1. This results from the requirement for muons to have $p \gtrsim 3\,\mathrm{GeV}/c$ to reach the muon system. Smaller reductions of the signal efficiency also arise from the p_T requirement of the hardware trigger and the impact parameter requirements on the $\mu^\pm$ in the selection.

For the decay $B^+ \to K^+\mu^+\mu^-$, the $\overline{D}^0$ veto described in section 3 introduces an additional bias to the angular acceptance: at a fixed value of q^2, there is a one-to-one correspondence between $\cos\theta_l$ and the reconstructed $\overline{D}^0$ mass, and the $\overline{D}^0$ veto therefore removes a narrow region of $\cos\theta_l$ in each q^2 bin. The $\overline{D}^0$ veto results in the dip in the
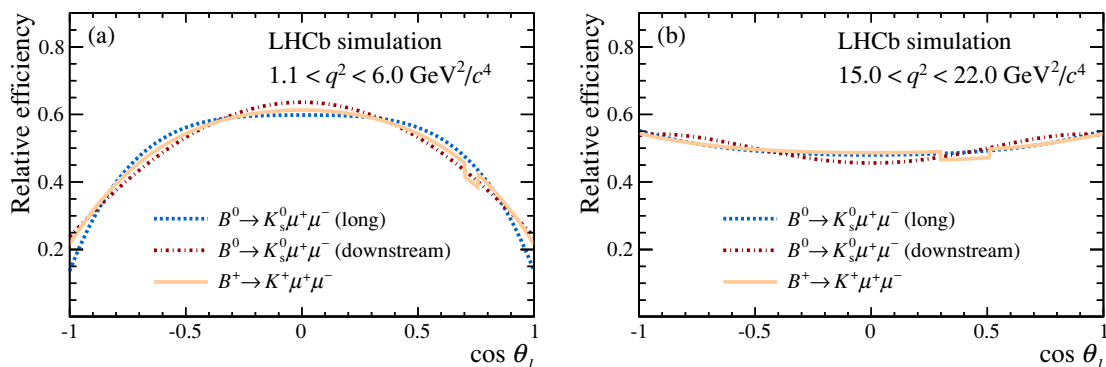
Figure 1. Angular acceptance as derived from simulation in the dimuon mass squared ranges (a) $1.1 < q^2 < 6.0 \,\mathrm{GeV}^2/c^4$ and (b) $15.0 < q^2 < 22.0 \,\mathrm{GeV}^2/c^4$. The dip in the acceptance for $B^+ \to K^+ \mu^+ \mu^-$ decays results from the veto used to reject $B^+ \to \overline{D}^0 \pi^+$ decays (see text). The acceptance is normalised to unit area to allow a comparison of the shape of the distributions.

acceptance seen in figure 1. The impact of the veto is approximated as a step function in the acceptance model and determined using a SM-like sample of simulated events.

5 Angular analysis

The $m(K^+\mu^+\mu^-)$ and $m(K_{\rm S}^0\mu^+\mu^-)$ invariant mass distributions of candidates that pass the full selection procedure are shown in figure 2, for two q^2 intervals. The long and downstream categories are combined for the decay $B^0 \to K_{\rm S}^0\mu^+\mu^-$. The angular distribution of the candidates is shown in figure 3.

For the $B^+ \to K^+\mu^+\mu^-$ decay, $A_{\rm FB}$ and $F_{\rm H}$ are determined by performing an unbinned maximum likelihood fit to the $m(K^+\mu^+\mu^-)$ and $\cos\theta_l$ distributions of the candidates in bins of q^2. The signal angular distribution is described by eq. (1.1), multiplied by the acceptance distribution described in section 4. The signal mass distribution is parameterised by the sum of two Gaussian functions with power-law tails, with common most probable values and common tail parameters, but different widths. The parameters of the these signal functions are obtained fitting the $m(K^+\mu^+\mu^-)$ distribution of $B^+ \to J/\psi\,K^+$ candidates in data. The peak position and width parameters are then corrected, using simulated events, to account for kinematic differences between the decays $B^+ \to K^+\mu^+\mu^-$ and $B^+ \to J/\psi\,K^+$. The $m(K^+\mu^+\mu^-)$ distribution of the combinatorial background is parameterised by a falling exponential function. Its angular distribution is parameterised by a third-order polynomial function multiplied by the same angular acceptance function used for the signal.

Decays of B^0 and $\overline{B}^0$ mesons to the $K_{\rm S}^0\mu^+\mu^-$ final state cannot be separated based on the final-state particles. The angular distribution of $|\cos\theta_l|$ is described by eq. (1.2), which depends only on $F_{\rm H}$. Simultaneous unbinned maximum likelihood fits are then performed to the $|\cos\theta_l|$ and $m(K_{\rm S}^0\mu^+\mu^-)$ distributions of the two categories of $K_{\rm S}^0$ meson (long and downstream). The only parameter that is common between the two simultaneous fits is $F_{\rm H}$. The $m(K_{\rm S}^0\mu^+\mu^-)$ shape parameters of the two categories are determined in the same way as that of the decay $B^+ \to K^+\mu^+\mu^-$, using $B^0 \to J/\psi\,K_{\rm S}^0$ decays. Information on the angular
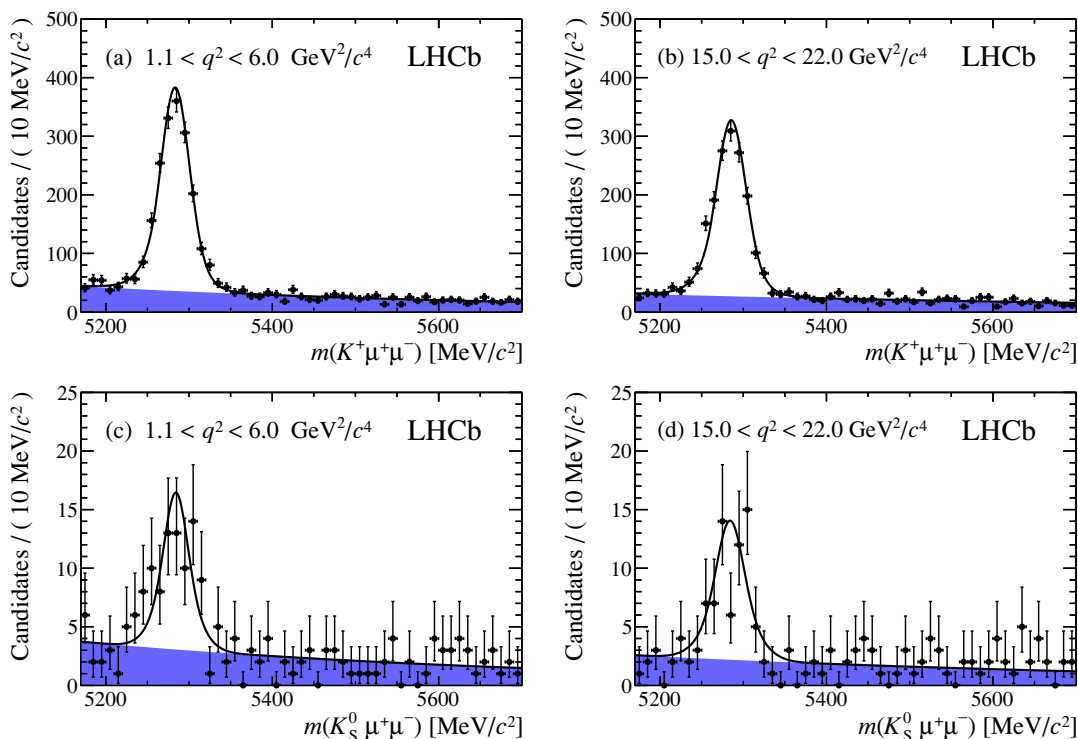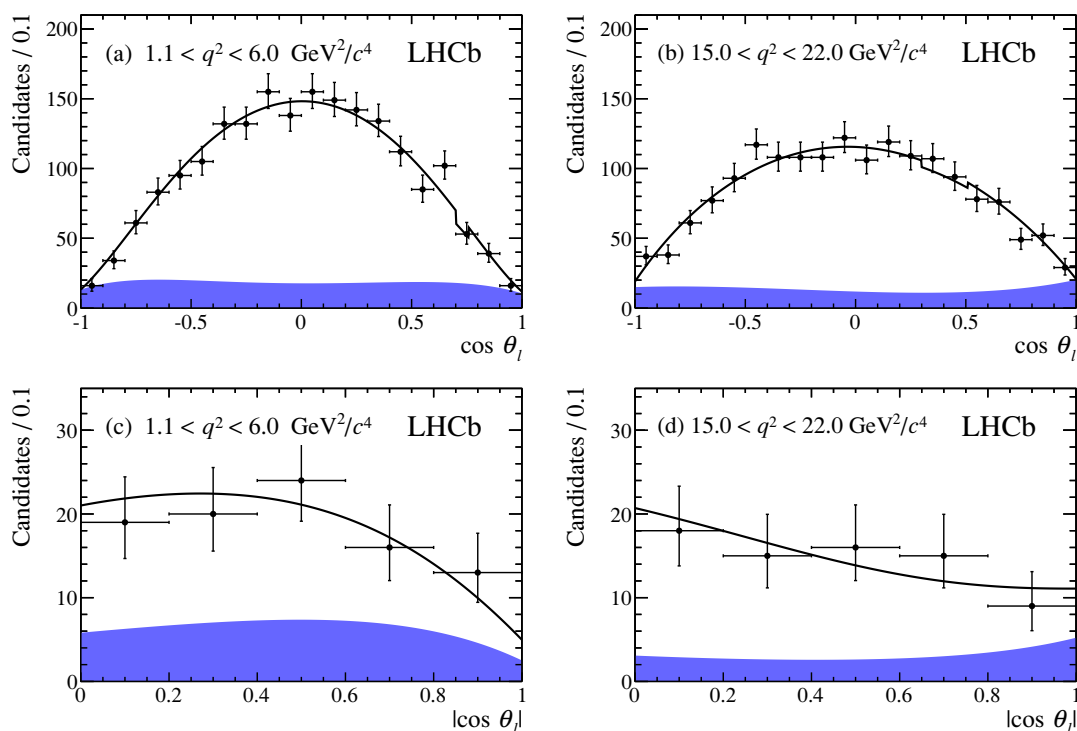
Figure 2. Top, reconstructed mass of $B^+ \to K^+\mu^+\mu^-$ candidates in the ranges (a) $1.1 < q^2 < 6.0\,\mathrm{GeV}^2/c^4$ and (b) $15.0 < q^2 < 22.0\,\mathrm{GeV}^2/c^4$. Bottom, reconstructed mass of $B^0 \to K_S^0\mu^+\mu^-$ candidates in the ranges (c) $1.1 < q^2 < 6.0\,\mathrm{GeV}^2/c^4$ and (d) $15.0 < q^2 < 22.0\,\mathrm{GeV}^2/c^4$. The data are overlaid with the result of the fit described in the text. The long and downstream K_S^0 categories are combined for presentation purposes. The shaded region indicates the background contribution in the fit.

shape of the background in the likelihood fit is obtained from the upper mass sideband, $5350 < m(K_S^0\mu^+\mu^-) < 5700\,\mathrm{MeV}/c^2$. For candidates in the long K_S^0 category, the number of candidates in the sideband is so small that the shape is assumed to be uniform. For the downstream category, the shape is parameterised by a second-order polynomial. The signal and background angular distributions are then both multiplied by the signal angular acceptance distribution. The $m(K_S^0\mu^+\mu^-)$ distribution of the background candidates is parameterised by a falling exponential function.

The likelihood fits for the $B^+ \to K^+\mu^+\mu^-$ decay and the two categories of K_S^0 meson in the $B^0 \to K_S^0\mu^+\mu^-$ decay are performed in two dimensions, treating $m(K^+\mu^+\mu^-)$ and $\cos\theta_l$ as independent variables. In total, there are 4746 ± 81 reconstructed signal candidates for the $B^+ \to K^+\mu^+\mu^-$ decay and 176 ± 17 for the $B^0 \to K_S^0\mu^+\mu^-$ decay, summing the yields of the individual q^2 bins.

6 Results

For the decay $B^+ \to K^+\mu^+\mu^-$, the results are presented as two-dimensional confidence regions for A_{FB} and F_{H} and as one-dimensional 68% confidence intervals for A_{FB} and F_{H}. The two-dimensional confidence regions demonstrate the correlation between A_{FB} and F_{H}

Figure 3. Top, angular distribution of $B^+ \rightarrow K^+\mu^+\mu^-$ candidates with (a) $1.1 < q^2 < 6.0\,\mathrm{GeV}^2/c^4$ and (b) $15.0 < q^2 < 22.0\,\mathrm{GeV}^2/c^4$. Bottom, angular distribution of $B^0 \rightarrow K_\mathrm{S}^0\mu^+\mu^-$ candidates with (c) $1.1 < q^2 < 6.0\,\mathrm{GeV}^2/c^4$ and (d) $15.0 < q^2 < 22.0\,\mathrm{GeV}^2/c^4$. Only candidates with a reconstructed mass within $\pm 50\,\mathrm{MeV}/c^2$ of the known B^+ or B^0 mass are shown. The data are overlaid with the result of the fit described in the text. The long and downstream K_S^0 categories are combined for presentation purposes. The shaded region indicates the background contribution in the fit.

arising from eq. (1.1). The one-dimensional intervals are intended for illustration purposes only. Two-dimensional confidence regions, for the q^2 ranges $1.1 < q^2 < 6.0\,\mathrm{GeV}^2/c^4$ and $15.0 < q^2 < 22.0\,\mathrm{GeV}^2/c^4$ are shown in figure 4; the other q^2 bins are provided in the appendix, with the numerical values available in the attachment.[3] The one-dimensional confidence intervals for $B^+ \rightarrow K^+\mu^+\mu^-$ decays are shown in figure 5 and given in table 1. The result of the fits to $|\cos\theta_l|$ for the decay $B^0 \rightarrow K_\mathrm{S}^0\mu^+\mu^-$ are shown in figure 6 and given in table 2. Results are presented in 17 (5) bins of q^2 for the $B^+ \rightarrow K^+\mu^+\mu^-$ ($B^0 \rightarrow K_\mathrm{S}^0\mu^+\mu^-$) decay. They are also presented in two wide bins of q^2: one at low hadronic recoil above the open charm threshold and one at large recoil, below the J/ψ meson mass.

The confidence intervals on F_H and A_FB are estimated using the Feldman-Cousins technique [23]. Nuisance parameters are incorporated using the so-called plug-in method [24]. At each value of F_H and A_FB considered, the maximum likelihood estimate of the nuisance parameters in data is used when generating the pseudoexperiments. For the $B^+ \rightarrow K^+\mu^+\mu^-$ decay, A_FB (F_H) is treated as if it were a nuisance parameter when determining the one-dimensional confidence interval on F_H (A_FB). The physical boundaries, described in

---

[3]Data files are provided as supplementary material and are available at this article's web page.
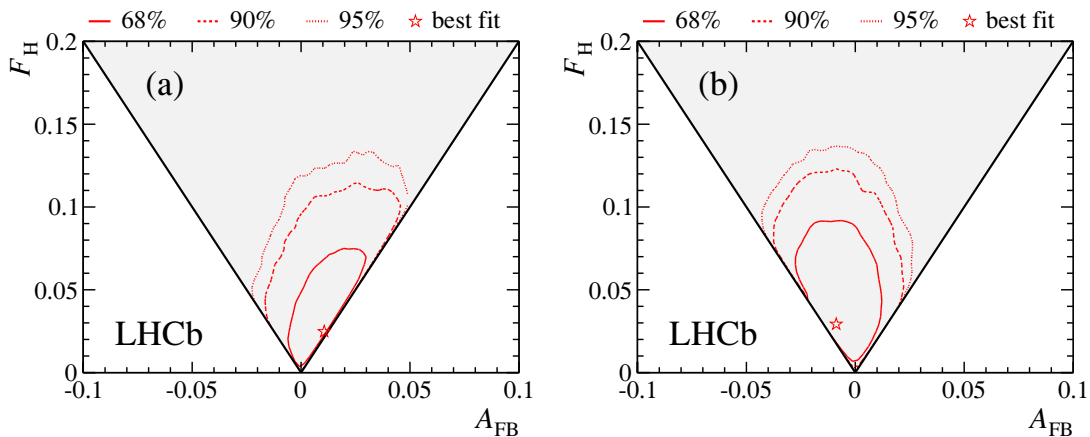
Figure 4. Two-dimensional confidence regions for $A_{\rm FB}$ and $F_{\rm H}$ for the decay $B^+ \to K^+ \mu^+ \mu^-$ in the q^2 ranges (a) $1.1 < q^2 < 6.0\,{\rm GeV}^2/c^4$ and (b) $15.0 < q^2 < 22.0\,{\rm GeV}^2/c^4$. The confidence intervals are determined using the Feldman-Cousins technique. The shaded (triangular) region illustrates the range of $A_{\rm FB}$ and $F_{\rm H}$ over which the signal angular distribution remains positive in all regions of phase-space.

section 1, are accounted for in the generation of pseudoexperiments when building the confidence belts. Due to the requirement that $|A_{\rm FB}| \leq F_{\rm H}/2$, statistical fluctuations of events in $\cos \theta_l$ have a tendency to drive $F_{\rm H}$ to small positive values in the pseudoexperiments.

For the $B^0 \to K_S^0 \mu^+ \mu^-$ decay, fits are also performed to $\cos \theta_l$ allowing for a non-zero $A_{\rm FB}$ using eq. (1.1). The value of $A_{\rm FB}$ determined by these fits is consistent with zero, as expected, and the best fit value of $F_{\rm H}$ compatible with that of the baseline fit.

The data for $F_{\rm H}$ in figures 5 and 6 are superimposed with theoretical predictions from ref. [25]. In the low q^2 region, these predictions rely on the QCD factorisation approaches from ref. [2], which lose accuracy when the dimuon mass approaches the J/ψ mass. In the high q^2 region, an operator product expansion in the inverse b-quark mass, $1/m_b$, and in $1/\sqrt{q^2}$ is used based on ref. [26]. This expansion is only valid above the open charm threshold. A dimensional estimate of the uncertainty associated with this expansion is discussed in ref. [27]. Form-factor calculations are taken from ref. [28]

Two classes of systematic uncertainty are considered for $A_{\rm FB}$ and $F_{\rm H}$: detector-related uncertainties that might affect the angular acceptance, and uncertainties related to the angular distribution of the background.

The samples of simulated events used to determine the detector acceptance are corrected to match the performance observed in data by degrading the impact parameter resolution on the kaon and muons by 20%, re-weighting candidates to reproduce the kinematic distribution of B^+ candidates in the data and re-weighting candidates to account for differences in tracking and particle-identification performance. Varying these corrections within their known uncertainties has a negligible impact on $A_{\rm FB}$ and $F_{\rm H}$ ($\lesssim 0.01$).

The acceptance as a function of $\cos \theta_l$ is determined from simulated events in each bin of q^2. This assumes that the distribution of events in q^2, within the q^2 bin, is the same in simulation and in data. To assess the systematic uncertainty arising from this assumption,
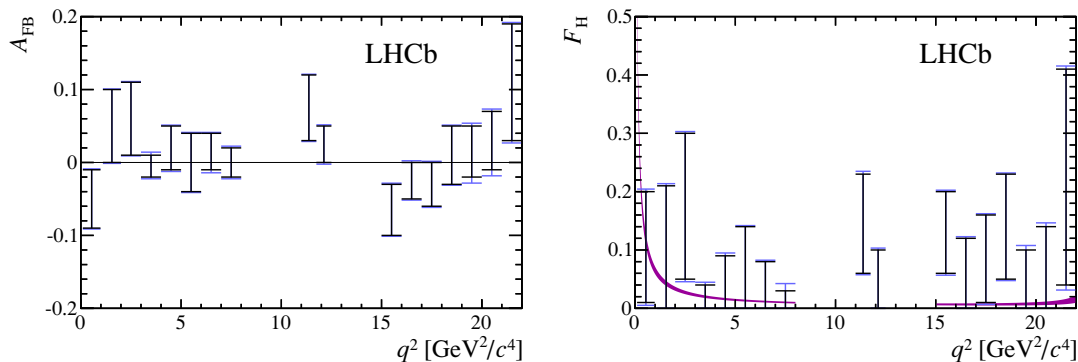
Figure 5. Dimuon forward-backward asymmetry, A_{FB}, and the parameter F_{H} for the decay $B^+ \to K^+\mu^+\mu^-$ as a function of the dimuon invariant mass squared, q^2. The inner horizontal bars indicate the one-dimensional 68% confidence intervals. The outer vertical bars include contributions from systematic uncertainties (described in the text). The confidence intervals for F_{H} are overlaid with the SM theory prediction (narrow band). Data are not presented for the regions around the J/ψ and $\psi(2S)$ resonances.
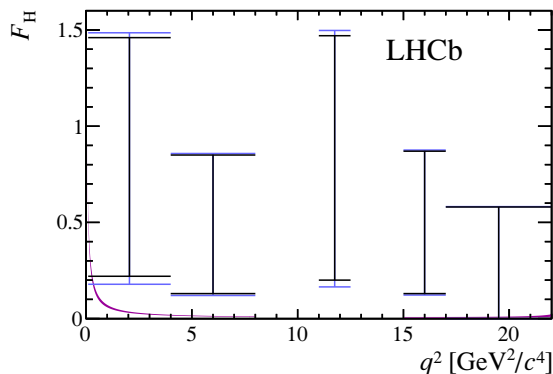
Figure 6. Results for the parameter F_{H} for the decay $B^0 \to K^0_{\mathrm{S}}\mu^+\mu^-$ as a function of the dimuon invariant mass squared, q^2. The inner horizontal bars indicate the one-dimensional 68% confidence intervals. The outer vertical bars include contributions from systematic uncertainties (described in the text). The confidence intervals are overlaid with the SM theory prediction (narrow band). Data are not presented for the regions around the J/ψ and $\psi(2S)$ resonances.

the acceptance as a function of $\cos\theta_l$ is determined separately for simulated events in the lower and upper half of the q^2 bin, and the average acceptance correction for the bin is re-computed varying the relative contributions from the lower and upper half by 20%. This level of variation covers any observed difference between the differential decay rate as a function of q^2 in data and in simulation and introduces an uncertainty at the level of 0.01 on A_{FB} and F_{H}.

In order to investigate the background modelling, the multivariate selection requirements are relaxed. With the increased level of background in the upper mass sideband, an alternative background model of a fourth-order polynomial is derived. Pseudoexperiments are then generated that explore the differences between the A_{FB} or F_{H} values obtained with

$q^2(\text{GeV}^2/c^4)$	F_H (stat)	F_H (syst)	A_{FB} (stat)	A_{FB} (syst)
$0.10 - 0.98$	$[+0.01, +0.20]$	± 0.03	$[-0.09, -0.01]$	± 0.01
$1.10 - 2.00$	$[+0.00, +0.21]$	± 0.03	$[+0.00, +0.10]$	± 0.01
$2.00 - 3.00$	$[+0.05, +0.30]$	± 0.03	$[+0.01, +0.11]$	± 0.01
$3.00 - 4.00$	$[\ \ 0.00, +0.04]$	± 0.02	$[-0.02, +0.01]$	± 0.01
$4.00 - 5.00$	$[\ \ 0.00, +0.09]$	± 0.03	$[-0.01, +0.05]$	± 0.01
$5.00 - 6.00$	$[\ \ 0.00, +0.14]$	± 0.02	$[-0.04, +0.04]$	± 0.01
$6.00 - 7.00$	$[\ \ 0.00, +0.08]$	± 0.02	$[-0.01, +0.04]$	± 0.01
$7.00 - 8.00$	$[\ \ 0.00, +0.03]$	± 0.03	$[-0.02, +0.02]$	± 0.01
$11.00 - 11.75$	$[+0.06, +0.23]$	± 0.03	$[+0.03, +0.12]$	± 0.01
$11.75 - 12.50$	$[+0.00, +0.10]$	± 0.02	$[+0.00, +0.05]$	± 0.01
$15.00 - 16.00$	$[+0.06, +0.20]$	± 0.02	$[-0.10, -0.03]$	± 0.01
$16.00 - 17.00$	$[+0.00, +0.12]$	± 0.02	$[-0.05, +0.00]$	± 0.01
$17.00 - 18.00$	$[+0.01, +0.16]$	± 0.02	$[-0.06, +0.00]$	± 0.01
$18.00 - 19.00$	$[+0.05, +0.23]$	± 0.02	$[-0.03, +0.05]$	± 0.01
$19.00 - 20.00$	$[\ \ 0.00, +0.10]$	± 0.04	$[-0.02, +0.05]$	± 0.02
$20.00 - 21.00$	$[\ \ 0.00, +0.14]$	± 0.04	$[-0.01, +0.07]$	± 0.02
$21.00 - 22.00$	$[+0.04, +0.41]$	± 0.05	$[+0.03, +0.19]$	± 0.02
$1.10 - 6.00$	$[\ \ 0.00, +0.06]$	± 0.02	$[-0.01, +0.02]$	± 0.01
$15.00 - 22.00$	$[\ \ 0.00, +0.07]$	± 0.02	$[-0.03, +0.00]$	± 0.01

Table 1. Forward-backward asymmetry, A_{FB}, and F_H for the decay $B^+ \to K^+ \mu^+ \mu^-$ in the q^2 bins used in this analysis. These parameters are also given in a wide bin at large $(1.1 < q^2 < 6.0\,\text{GeV}^2/c^4)$ and low $(15.0 < q^2 < 22.0\,\text{GeV}^2/c^4)$ hadronic recoil. The column labelled *stat* is the 68% statistical confidence interval on F_H (A_{FB}) when treating A_{FB} (F_H) as a nuisance parameter. The column labelled *syst* is the systematic uncertainty.

$q^2(\text{GeV}^2/c^4)$	F_H (stat)	F_H (syst)
$0.1 - 4.0$	$[+0.22, +1.46]$	± 0.28
$4.0 - 8.0$	$[+0.13, +0.85]$	± 0.08
$11.0 - 12.5$	$[+0.20, +1.47]$	± 0.20
$15.0 - 17.0$	$[+0.12, +0.77]$	± 0.07
$17.0 - 22.0$	$[\ \ 0.00, +0.58]$	± 0.04
$1.1 - 6.0$	$[+0.32, +1.24]$	± 0.09
$15.0 - 22.0$	$[+0.09, +0.59]$	± 0.03

Table 2. The 68% confidence interval on the parameter F_H for the decay $B^0 \to K^0_s \mu^+ \mu^-$ in q^2 bins. In addition to the narrow binning used in the analysis, results are also given in wide bins at large $(1.1 < q^2 < 6.0\,\text{GeV}^2/c^4)$ and low $(15.0 < q^2 < 22.0\,\text{GeV}^2/c^4)$ hadronic recoil. The column labelled *stat* is the 68% statistical confidence interval. The column labelled *syst* is the systematic uncertainty.

the default and the alternative background model. A systematic uncertainty is assigned based on the sum in quadrature of the root-mean-square of these differences and the mean bias. The method introduces an uncertainty at the level of 0.01 on A_{FB} and $0.02 - 0.05$ on F_{H} for the $B^+ \to K^+ \mu^+ \mu^-$ decay and $0.04 - 0.20$ for the $B^0 \to K^0_{\mathrm{S}} \mu^+ \mu^-$ decay.

The dependence of the one-dimensional A_{FB} (F_{H}) confidence interval on the assumed true value of the F_{H} (A_{FB}) nuisance parameter is negligible ($\lesssim 0.01$).

The fitting procedure for $B^+ \to K^+ \mu^+ \mu^-$ ($B^0 \to K^0_{\mathrm{S}} \mu^+ \mu^-$) decays is also tested using samples of $B^+ \to J/\psi K^+$ ($B^0 \to J/\psi K^0_{\mathrm{S}}$) decays where $A_{\mathrm{FB}} = F_{\mathrm{H}} = 0$, due to the vector nature of the J/ψ meson. These samples are more than one hundred times larger than the signal samples. Tests are also performed splitting these samples into sub-samples of comparable size to the data sets in the individual q^2 bins. No indication of any bias is seen in the fitting procedure in either set of tests.

7 Conclusion

In summary, the angular distributions of charged and neutral $B \to K \mu^+ \mu^-$ decays are studied using a data set, corresponding to an integrated luminosity of $3\,\mathrm{fb}^{-1}$, collected by the LHCb experiment. The angular distribution of the decays is parameterised in terms of the forward-backward asymmetry of the decay, A_{FB}, and a parameter F_{H}, which is a measure of the contribution from (pseudo)scalar and tensor amplitudes to the decay width.

The measurements of A_{FB} and F_{H} presented for the decays $B^+ \to K^+ \mu^+ \mu^-$ and $B^0 \to K^0_{\mathrm{S}} \mu^+ \mu^-$ are the most precise to date. They are consistent with SM predictions ($A_{\mathrm{FB}} \approx 0$ and $F_{\mathrm{H}} \approx 0$) in every bin of q^2. The results are also compatible between the decays $B^+ \to K^+ \mu^+ \mu^-$ and $B^0 \to K^0_{\mathrm{S}} \mu^+ \mu^-$. The largest difference with respect to the SM prediction is seen in the range $11.00 < q^2 < 11.75\,\mathrm{GeV}^2/c^4$ for the decay $B^+ \to K^+ \mu^+ \mu^-$. Even in this bin, the SM point is included at 95% confidence level when taking into account the systematic uncertainties on the angular observables.

The results place constraints on (pseudo)scalar and tensor amplitudes, which are vanishingly small in the SM but can be enhanced in many extensions of the SM. Pseudoscalar and scalar amplitudes were already highly constrained by measurements of the branching fraction of the decay $B^0_s \to \mu^+ \mu^-$ [29, 30]. The results presented here, however, also rule out the possibility of large accidental cancellations between the left- and right-handed couplings of the (pseudo)scalar amplitudes to the $B^0_s \to \mu^+ \mu^-$ branching fraction. Tensor amplitudes were previously poorly constrained.

Acknowledgments

A Two-dimensional confidence intervals

(a) $0.10 < q^2 < 0.98\,\mathrm{GeV}^2/c^4$

(b) $1.10 < q^2 < 2.00\,\mathrm{GeV}^2/c^4$

(c) $2.00 < q^2 < 3.00\,\mathrm{GeV}^2/c^4$
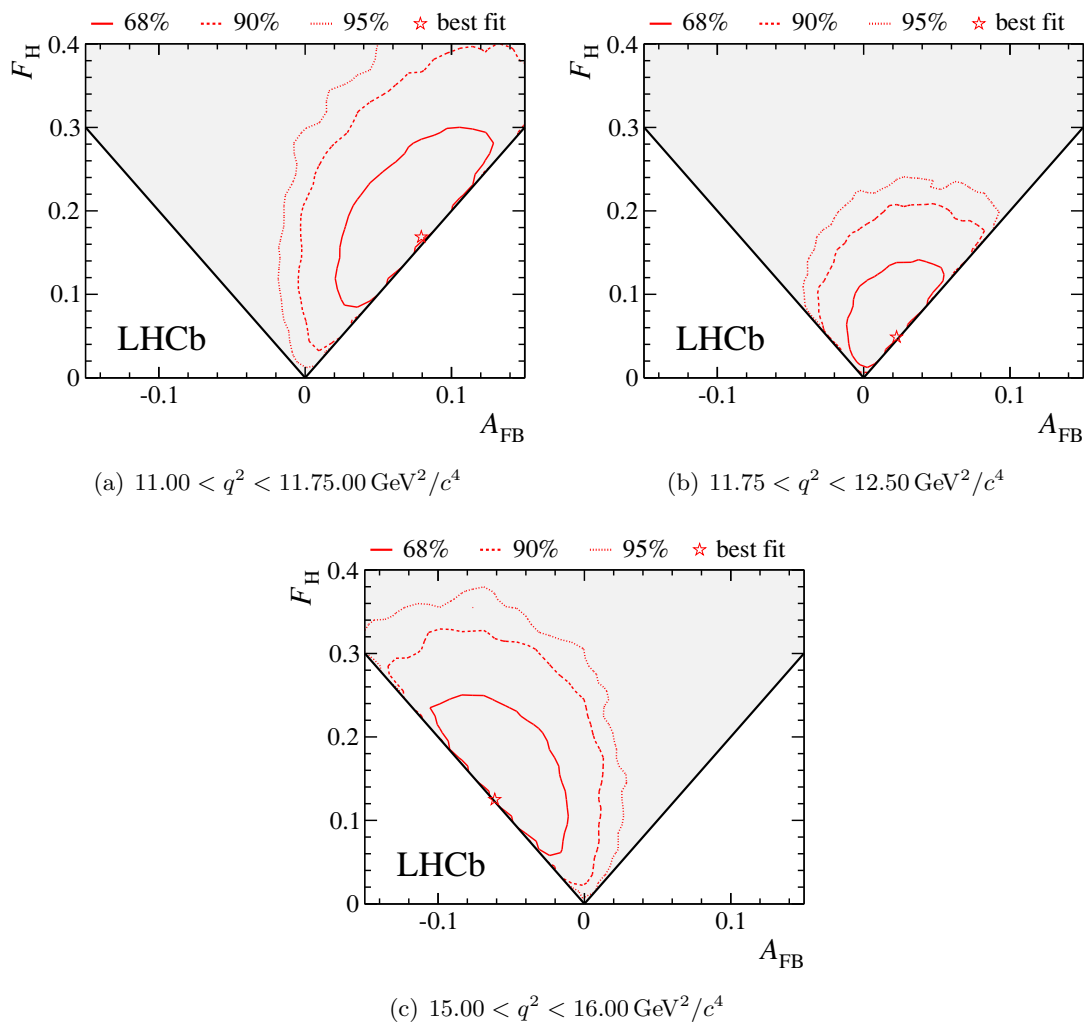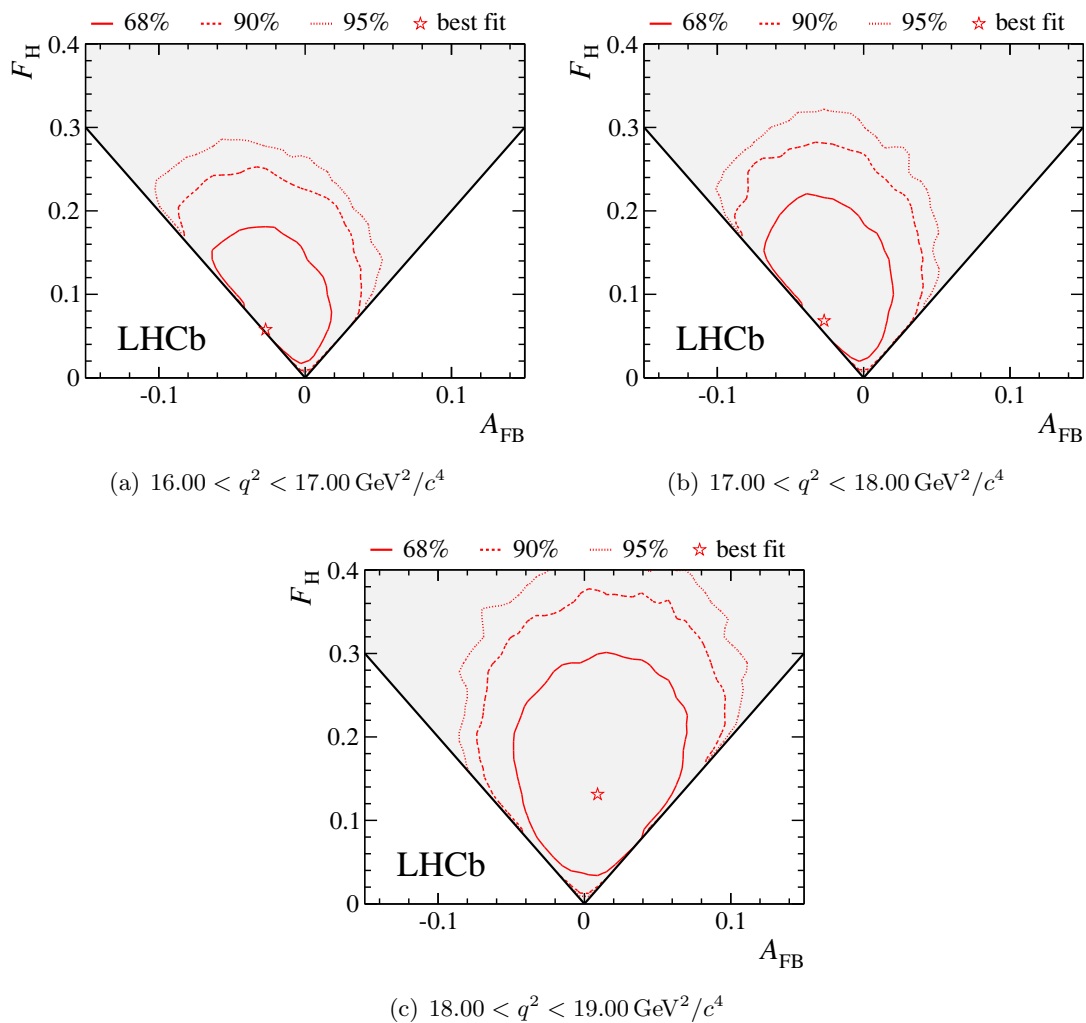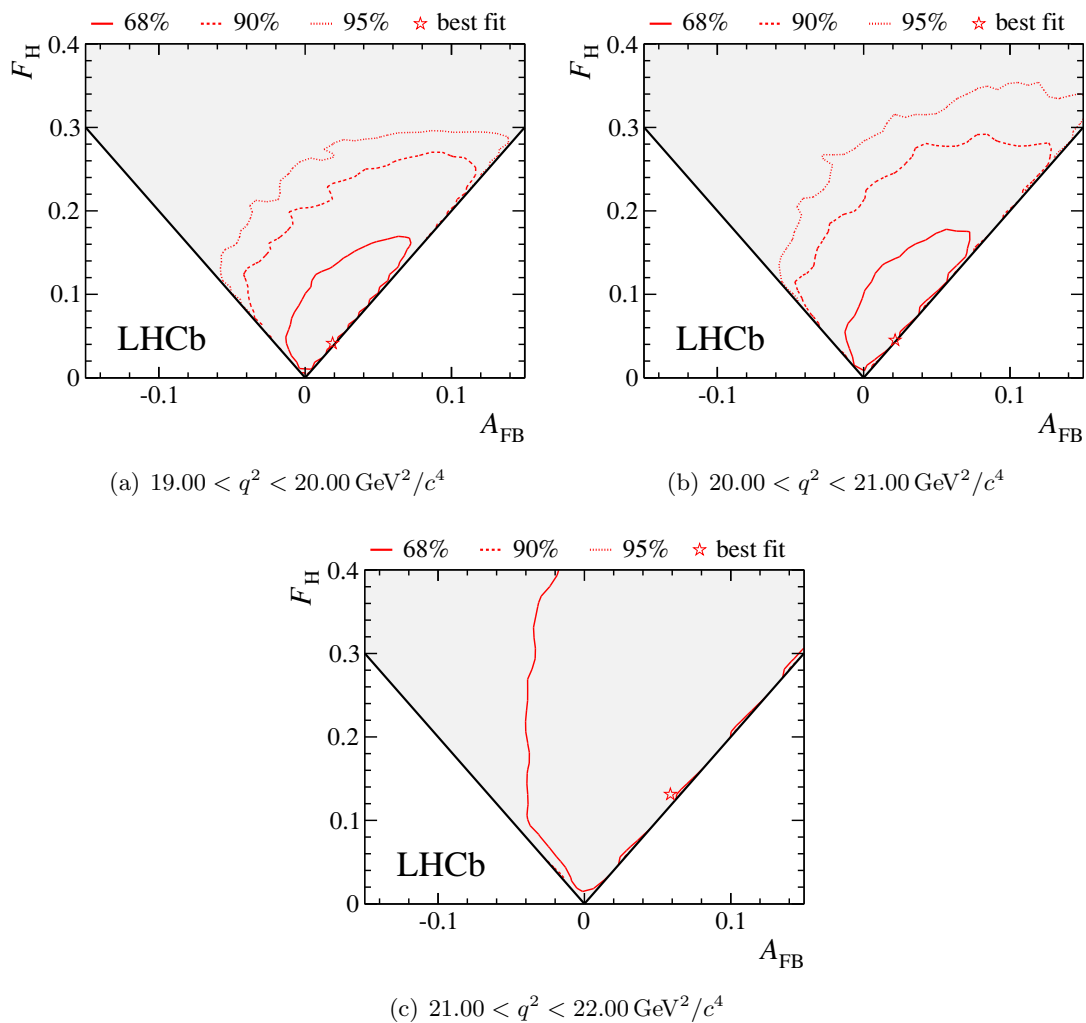
(d) $3.00 < q^2 < 4.00\,\mathrm{GeV}^2/c^4$

Figure 7. Two-dimensional confidence regions for A_{FB} and F_{H} for the decay $B^+ \to K^+\mu^+\mu^-$ in the q^2 ranges (a) $0.10 < q^2 < 0.98\,\mathrm{GeV}^2/c^4$, (b) $1.10 < q^2 < 2.00\,\mathrm{GeV}^2/c^4$, (c) $2.00 < q^2 < 3.00\,\mathrm{GeV}^2/c^4$ and (d) $3.00 < q^2 < 4.00\,\mathrm{GeV}^2/c^4$. The confidence intervals are determined using the Feldman-Cousins technique and are purely statistical. The shaded (triangular) region illustrates the range of A_{FB} and F_{H} over which the signal angular distribution remains positive in all regions of phase-space.
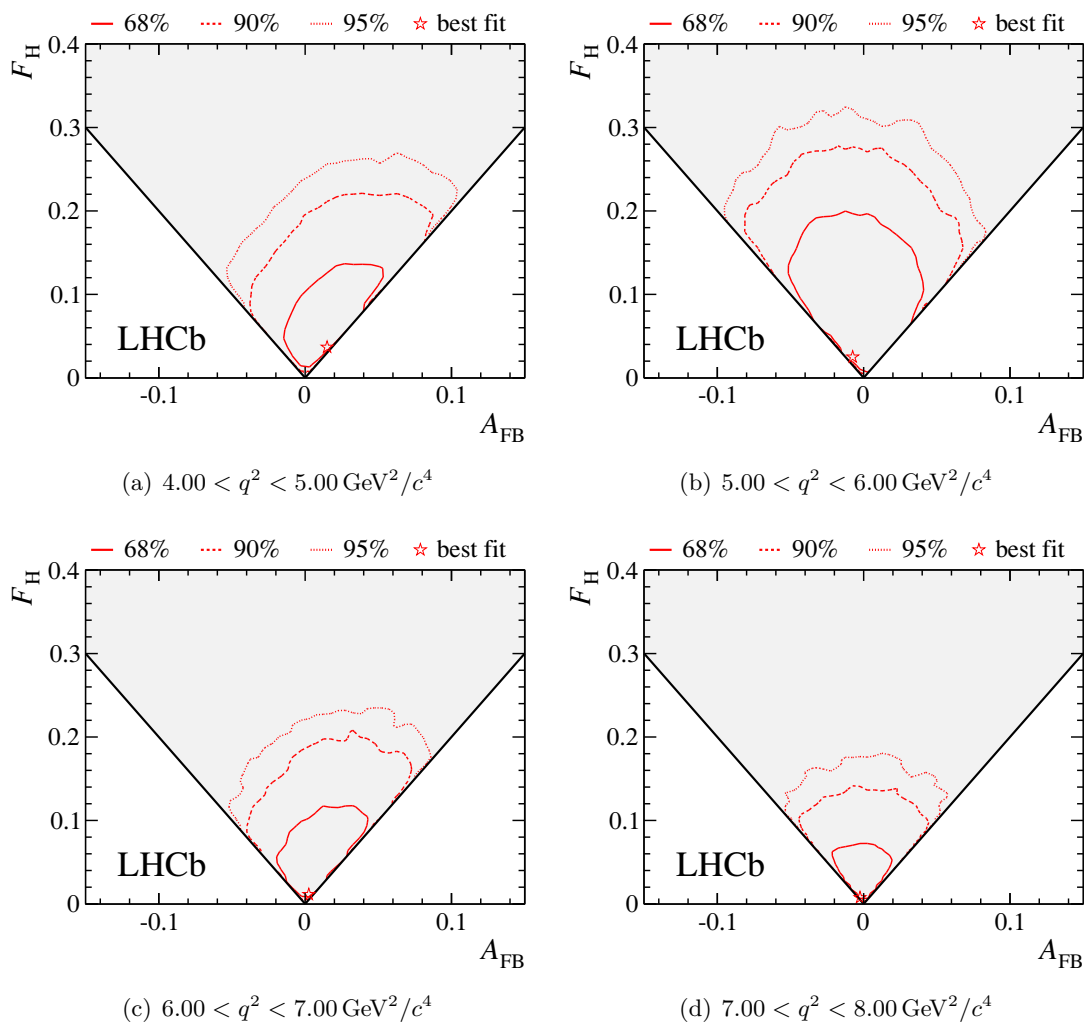
Figure 8. Two-dimensional confidence regions for A_{FB} and F_H for the decay $B^+ \rightarrow K^+ \mu^+ \mu^-$ in the q^2 ranges (a) $4.00 < q^2 < 5.00\,\mathrm{GeV}^2/c^4$, (b) $5.00 < q^2 < 6.00\,\mathrm{GeV}^2/c^4$, (c) $6.00 < q^2 < 7.00\,\mathrm{GeV}^2/c^4$ and (d) $7.00 < q^2 < 8.00\,\mathrm{GeV}^2/c^4$. The confidence intervals are determined using the Feldman-Cousins technique and are purely statistical. The shaded (triangular) region illustrates the range of A_{FB} and F_H over which the signal angular distribution remains positive in all regions of phase-space.

(a) $11.00 < q^2 < 11.75.00\,\mathrm{GeV}^2/c^4$

(b) $11.75 < q^2 < 12.50\,\mathrm{GeV}^2/c^4$

(c) $15.00 < q^2 < 16.00\,\mathrm{GeV}^2/c^4$

Figure 9. Two-dimensional confidence regions for A_{FB} and F_{H} for the decay $B^+ \to K^+\mu^+\mu^-$ in the q^2 ranges (a) $11.00 < q^2 < 11.75\,\mathrm{GeV}^2/c^4$, (b) $11.75 < q^2 < 12.50\,\mathrm{GeV}^2/c^4$ and (c) $15.00 < q^2 < 16.00\,\mathrm{GeV}^2/c^4$. The confidence intervals are determined using the Feldman-Cousins technique and are purely statistical. The shaded (triangular) region illustrates the range of A_{FB} and F_{H} over which the signal angular distribution remains positive in all regions of phase-space.

Figure 10. Two-dimensional confidence regions for A_{FB} and F_H for the decay $B^+ \rightarrow K^+ \mu^+ \mu^-$ in the q^2 ranges (a) $16.00 < q^2 < 17.00\,\text{GeV}^2/c^4$, (b) $17.00 < q^2 < 18.00\,\text{GeV}^2/c^4$ and (c) $18.00 < q^2 < 19.00\,\text{GeV}^2/c^4$. The confidence intervals are determined using the Feldman-Cousins technique and are purely statistical. The shaded (triangular) region illustrates the range of A_{FB} and F_H over which the signal angular distribution remains positive in all regions of phase-space.

Figure 11. Two-dimensional confidence regions for A_{FB} and F_H for the decay $B^+ \to K^+\mu^+\mu^-$ in the q^2 ranges (a) $19.00 < q^2 < 20.00\,\mathrm{GeV}^2/c^4$, (b) $20.00 < q^2 < 21.00\,\mathrm{GeV}^2/c^4$ and (c) $21.00 < q^2 < 22.00\,\mathrm{GeV}^2/c^4$. The confidence intervals are determined using the Feldman-Cousins technique and are purely statistical. The shaded (triangular) region illustrates the range of A_{FB} and F_H over which the signal angular distribution remains positive in all regions of phase-space.

References

[1] A.K. Alok, A. Dighe and S.U. Sankar, *Large forward-backward asymmetry in $B \to K\mu^+\mu^-$ from new physics tensor operators*, *Phys. Rev.* **D 78** (2008) 114025 [`arXiv:0810.3779`] [ɪɴSPIRE].

[2] C. Bobeth, G. Hiller and G. Piranishvili, *Angular distributions of $\bar{B} \to K\bar{l}l$ decays*, *JHEP* **12** (2007) 040 [`arXiv:0709.4174`] [ɪɴSPIRE].

[3] BaBar collaboration, B. Aubert et al., *Measurements of branching fractions, rate asymmetries and angular distributions in the rare decays $B \to K\ell^+\ell^-$ and $B \to K^*\ell^+\ell^-$*, *Phys. Rev.* **D 73** (2006) 092001 [`hep-ex/0604007`] [ɪɴSPIRE].

[4] BELLE collaboration, J.-T. Wei et al., *Measurement of the Differential Branching Fraction and Forward-Backword Asymmetry for $B \to K^{(*)}\ell^+\ell^-$*, *Phys. Rev. Lett.* **103** (2009) 171801 [`arXiv:0904.0770`] [ɪɴSPIRE].

[5] CDF collaboration, T. Aaltonen et al., *Measurements of the Angular Distributions in the Decays $B \to K^{(*)}\mu^+\mu^-$ at CDF*, *Phys. Rev. Lett.* **108** (2012) 081807 [`arXiv:1108.0695`] [ɪɴSPIRE].

[6] LHCb collaboration, *Differential branching fraction and angular analysis of the $B^+ \to K^+\mu^+\mu^-$ decay*, *JHEP* **02** (2013) 105 [`arXiv:1209.4284`] [ɪɴSPIRE].

[7] A. Ali, P. Ball, L.T. Handoko and G. Hiller, *A Comparative study of the decays $B \to (K, K^*)\ell^+\ell^-$ in standard model and supersymmetric theories*, *Phys. Rev.* **D 61** (2000) 074024 [`hep-ph/9910221`] [ɪɴSPIRE].

[8] LHCb collaboration, *The LHCb Detector at the LHC*, 2008 *JINST* **3** S08005 [ɪɴSPIRE].

[9] R. Arink et al., *Performance of the LHCb Outer Tracker*, 2014 *JINST* **9** P01002 [`arXiv:1311.3893`] [ɪɴSPIRE].

[10] LHCb RICH collaboration, *Performance of the LHCb RICH detector at the LHC*, *Eur. Phys. J.* **C 73** (2013) 2431 [`arXiv:1211.6759`] [ɪɴSPIRE].

[11] A.A. Alves Jr. et al., *Performance of the LHCb muon system*, 2013 *JINST* **8** P02022 [`arXiv:1211.1346`] [ɪɴSPIRE].

[12] T. Sjöstrand, S. Mrenna and P.Z. Skands, *PYTHIA 6.4 physics and manual*, *JHEP* **05** (2006) 026 [`hep-ph/0603175`] [ɪɴSPIRE].

[13] I. Belyaev et al., *Handling of the generation of primary events in* Gauss, *the LHCb simulation framework*, *IEEE Nucl. Sci. Symp. Conf. Rec. (NSS/MIC)* **2010** (2010) 1155.

[14] D.J. Lange, *The EvtGen particle decay simulation package*, *Nucl. Instrum. Meth.* **A 462** (2001) 152 [ɪɴSPIRE].

[15] P. Golonka and Z. Was, *PHOTOS Monte Carlo: A Precision tool for QED corrections in Z and W decays*, *Eur. Phys. J.* **C 45** (2006) 97 [`hep-ph/0506026`] [ɪɴSPIRE].

[16] GEANT4 collaboration, J. Allison et al., *Geant4 developments and applications*, *IEEE Trans. Nucl. Sci.* **53** (2006) 270.

[17] GEANT4 collaboration, S. Agostinelli et al., *GEANT4: a simulation toolkit*, *Nucl. Instrum. Meth.* **A 506** (2003) 250 [INSPIRE].

[18] M. Clemencic et al., *The LHCb simulation application, Gauss: design, evolution and experience*, *J. Phys. Conf. Ser.* **331** (2011) 032023 [INSPIRE].

[19] R. Aaij et al., *The LHCb Trigger and its Performance in 2011*, 2013 *JINST* **8** P04022 [arXiv:1211.3055] [INSPIRE].

[20] LHCb collaboration, *Observation of a resonance in $B^+ \to K^+\mu^+\mu^-$ decays at low recoil*, *Phys. Rev. Lett.* **111** (2013) 112003 [arXiv:1307.7595] [INSPIRE].

[21] L. Breiman, J.H. Friedman, R.A. Olshen and C.J. Stone, *Classification and regression trees*, Wadsworth international group, Belmont U.S.A. (1984).

[22] R.E. Schapire and Y. Freund, *A decision-theoretic generalization of on-line learning and an application to boosting*, *J. Comp. Syst. Sci.* **55** (1997) 119.

[23] G.J. Feldman and R.D. Cousins, *Unified approach to the classical statistical analysis of small signals*, *Phys. Rev.* **D 57** (1998) 3873 [physics/9711021] [INSPIRE].

[24] B. Sen, M. Walker and M. Woodroofe, *On the unified method with nuisance parameters*, *Statistica Sinica* **19** (2009) 301.

[25] C. Bobeth, G. Hiller, D. van Dyk and C. Wacker, *The decay $B \to K\ell^+\ell^-$ at low hadronic recoil and model-independent $\Delta B = 1$ constraints*, *JHEP* **01** (2012) 107 [arXiv:1111.2558] [INSPIRE].

[26] B. Grinstein and D. Pirjol, *Exclusive rare $B \to K^*\ell^+\ell^-$ decays at low recoil: controlling the long-distance effects*, *Phys. Rev.* **D 70** (2004) 114005 [hep-ph/0404250] [INSPIRE].

[27] U. Egede, T. Hurth, J. Matias, M. Ramon and W. Reece, *New observables in the decay mode $\bar{B}_d \to \bar{K}^{*0}\ell^+\ell^-$*, *JHEP* **11** (2008) 032 [arXiv:0807.2589] [INSPIRE].

[28] A. Khodjamirian, T. Mannel, A.A. Pivovarov and Y.-M. Wang, *Charm-loop effect in $B \to K^{(*)}\ell^+\ell^-$ and $B \to K^*\gamma$*, *JHEP* **09** (2010) 089 [arXiv:1006.4945] [INSPIRE].

[29] LHCb collaboration, *Measurement of the $B_s^0 \to \mu^+\mu^-$ branching fraction and search for $B^0 \to \mu^+\mu^-$ decays at the LHCb experiment*, *Phys. Rev. Lett.* **111** (2013) 101805 [arXiv:1307.5024] [INSPIRE].

[30] CMS collaboration, *Measurement of the $B_s^0 \to \mu^+\mu^-$ branching fraction and search for $B^0 \to \mu^+\mu^-$ with the CMS Experiment*, *Phys. Rev. Lett.* **111** (2013) 101804 [arXiv:1307.5025] [INSPIRE].

The LHCb collaboration

R. Aaij[41], B. Adeva[37], M. Adinolfi[46], A. Affolder[52], Z. Ajaltouni[5], J. Albrecht[9], F. Alessio[38], M. Alexander[51], S. Ali[41], G. Alkhazov[30], P. Alvarez Cartelle[37], A.A. Alves Jr[25,38], S. Amato[2], S. Amerio[22], Y. Amhis[7], L. An[3], L. Anderlini[17,g], J. Anderson[40], R. Andreassen[57], M. Andreotti[16,f], J.E. Andrews[58], R.B. Appleby[54], O. Aquines Gutierrez[10], F. Archilli[38], A. Artamonov[35], M. Artuso[59], E. Aslanides[6], G. Auriemma[25,n], M. Baalouch[5], S. Bachmann[11], J.J. Back[48], A. Badalov[36], V. Balagura[31], W. Baldini[16], R.J. Barlow[54], C. Barschel[38], S. Barsuk[7], W. Barter[47], V. Batozskaya[28], Th. Bauer[41], A. Bay[39], J. Beddow[51], F. Bedeschi[23], I. Bediaga[1], S. Belogurov[31], K. Belous[35], I. Belyaev[31], E. Ben-Haim[8], G. Bencivenni[18], S. Benson[50], J. Benton[46], A. Berezhnoy[32], R. Bernet[40], M.-O. Bettler[47], M. van Beuzekom[41], A. Bien[11], S. Bifani[45], T. Bird[54], A. Bizzeti[17,i], P.M. Bjørnstad[54], T. Blake[48], F. Blanc[39], J. Blouw[10], S. Blusk[59], V. Bocci[25], A. Bondar[34], N. Bondar[30,38], W. Bonivento[15,38], S. Borghi[54], A. Borgia[59], M. Borsato[7], T.J.V. Bowcock[52], E. Bowen[40], C. Bozzi[16], T. Brambach[9], J. van den Brand[42], J. Bressieux[39], D. Brett[54], M. Britsch[10], T. Britton[59], N.H. Brook[46], H. Brown[52], A. Bursche[40], G. Busetto[22,q], J. Buytaert[38], S. Cadeddu[15], R. Calabrese[16,f], O. Callot[7], M. Calvi[20,k], M. Calvo Gomez[36,o], A. Camboni[36], P. Campana[18,38], D. Campora Perez[38], A. Carbone[14,d], G. Carboni[24,l], R. Cardinale[19,38,j], A. Cardini[15], H. Carranza-Mejia[50], L. Carson[50], K. Carvalho Akiba[2], G. Casse[52], L. Cassina[20], L. Castillo Garcia[38], M. Cattaneo[38], Ch. Cauet[9], R. Cenci[58], M. Charles[8], Ph. Charpentier[38], S.-F. Cheung[55], N. Chiapolini[40], M. Chrzaszcz[40,26], K. Ciba[38], X. Cid Vidal[38], G. Ciezarek[53], P.E.L. Clarke[50], M. Clemencic[38], H.V. Cliff[47], J. Closier[38], C. Coca[29], V. Coco[38], J. Cogan[6], E. Cogneras[5], P. Collins[38], A. Comerma-Montells[11], A. Contu[15,38], A. Cook[46], M. Coombes[46], S. Coquereau[8], G. Corti[38], M. Corvo[16,f], I. Counts[56], B. Couturier[38], G.A. Cowan[50], D.C. Craik[48], M. Cruz Torres[60], S. Cunliffe[53], R. Currie[50], C. D'Ambrosio[38], J. Dalseno[46], P. David[8], P.N.Y. David[41], A. Davis[57], K. De Bruyn[41], S. De Capua[54], M. De Cian[11], J.M. De Miranda[1], L. De Paula[2], W. De Silva[57], P. De Simone[18], D. Decamp[4], M. Deckenhoff[9], L. Del Buono[8], N. Déléage[4], D. Derkach[55], O. Deschamps[5], F. Dettori[42], A. Di Canto[38], H. Dijkstra[38], S. Donleavy[52], F. Dordei[11], M. Dorigo[39], A. Dosil Suárez[37], D. Dossett[48], A. Dovbnya[43], F. Dupertuis[39], P. Durante[38], R. Dzhelyadin[35], A. Dziurda[26], A. Dzyuba[30], S. Easo[49], U. Egede[53], V. Egorychev[31], S. Eidelman[34], S. Eisenhardt[50], U. Eitschberger[9], R. Ekelhof[9], L. Eklund[51,38], I. El Rifai[5], Ch. Elsasser[40], S. Esen[11], T. Evans[55], A. Falabella[16,f], C. Färber[11], C. Farinelli[41], S. Farry[52], D. Ferguson[50], V. Fernandez Albor[37], F. Ferreira Rodrigues[1], M. Ferro-Luzzi[38], S. Filippov[33], M. Fiore[16,f], M. Fiorini[16,f], M. Firlej[27], C. Fitzpatrick[38], T. Fiutowski[27], M. Fontana[10], F. Fontanelli[19,j], R. Forty[38], O. Francisco[2], M. Frank[38], C. Frei[38], M. Frosini[17,38,g], J. Fu[21,38], E. Furfaro[24,l], A. Gallas Torreira[37], D. Galli[14,d], S. Gallorini[22], S. Gambetta[19,j], M. Gandelman[2], P. Gandini[59], Y. Gao[3], J. Garofoli[59], J. Garra Tico[47], L. Garrido[36], C. Gaspar[38], R. Gauld[55], L. Gavardi[9], E. Gersabeck[11], M. Gersabeck[54], T. Gershon[48], Ph. Ghez[4], A. Gianelle[22], S. Giani'[39], V. Gibson[47], L. Giubega[29], V.V. Gligorov[38], C. Göbel[60], D. Golubkov[31], A. Golutvin[53,31,38], A. Gomes[1,a], H. Gordon[38], C. Gotti[20], M. Grabalosa Gándara[5], R. Graciani Diaz[36], L.A. Granado Cardoso[38], E. Graugés[36], G. Graziani[17], A. Grecu[29], E. Greening[55], S. Gregson[47], P. Griffith[45], L. Grillo[11], O. Grünberg[62], B. Gui[59], E. Gushchin[33], Yu. Guz[35,38], T. Gys[38], C. Hadjivasiliou[59], G. Haefeli[39], C. Haen[38], S.C. Haines[47], S. Hall[53], B. Hamilton[58], T. Hampson[46], X. Han[11], S. Hansmann-Menzemer[11], N. Harnew[55], S.T. Harnew[46], J. Harrison[54], T. Hartmann[62], J. He[38], T. Head[38], V. Heijne[41], K. Hennessy[52], P. Henrard[5], L. Henry[8], J.A. Hernando Morata[37], E. van Herwijnen[38], M. Heß[62], A. Hicheur[1], D. Hill[55], M. Hoballah[5], C. Hombach[54], W. Hulsbergen[41], P. Hunt[55], N. Hussain[55], D. Hutchcroft[52], D. Hynds[51], M. Idzik[27], P. Ilten[56], R. Jacobsson[38], A. Jaeger[11], J. Jalocha[55], E. Jans[41], P. Jaton[39],

A. Jawahery[58], M. Jezabek[26], F. Jing[3], M. John[55], D. Johnson[55], C.R. Jones[47], C. Joram[38], B. Jost[38], N. Jurik[59], M. Kaballo[9], S. Kandybei[43], W. Kanso[6], M. Karacson[38], T.M. Karbach[38], M. Kelsey[59], I.R. Kenyon[45], T. Ketel[42], B. Khanji[20], C. Khurewathanakul[39], S. Klaver[54], O. Kochebina[7], M. Kolpin[11], I. Komarov[39], R.F. Koopman[42], P. Koppenburg[41,38], M. Korolev[32], A. Kozlinskiy[41], L. Kravchuk[33], K. Kreplin[11], M. Kreps[48], G. Krocker[11], P. Krokovny[34], F. Kruse[9], M. Kucharczyk[20,26,38,k], V. Kudryavtsev[34], K. Kurek[28], T. Kvaratskheliya[31], V.N. La Thi[39], D. Lacarrere[38], G. Lafferty[54], A. Lai[15], D. Lambert[50], R.W. Lambert[42], E. Lanciotti[38], G. Lanfranchi[18], C. Langenbruch[38], B. Langhans[38], T. Latham[48], C. Lazzeroni[45], R. Le Gac[6], J. van Leerdam[41], J.-P. Lees[4], R. Lefèvre[5], A. Leflat[32], J. Lefrançois[7], S. Leo[23], O. Leroy[6], T. Lesiak[26], B. Leverington[11], Y. Li[3], M. Liles[52], R. Lindner[38], C. Linn[38], F. Lionetto[40], B. Liu[15], G. Liu[38], S. Lohn[38], I. Longstaff[51], J.H. Lopes[2], N. Lopez-March[39], P. Lowdon[40], H. Lu[3], D. Lucchesi[22,q], H. Luo[50], A. Lupato[22], E. Luppi[16,f], O. Lupton[55], F. Machefert[7], I.V. Machikhiliyan[31], F. Maciuc[29], O. Maev[30], S. Malde[55], G. Manca[15,e], G. Mancinelli[6], M. Manzali[16,f], J. Maratas[5], J.F. Marchand[4], U. Marconi[14], C. Marin Benito[36], P. Marino[23,s], R. Märki[39], J. Marks[11], G. Martellotti[25], A. Martens[8], A. Martín Sánchez[7], M. Martinelli[41], D. Martinez Santos[42], F. Martinez Vidal[64], D. Martins Tostes[2], A. Massafferri[1], R. Matev[38], Z. Mathe[38], C. Matteuzzi[20], A. Mazurov[16,f], M. McCann[53], J. McCarthy[45], A. McNab[54], R. McNulty[12], B. McSkelly[52], B. Meadows[57,55], F. Meier[9], M. Meissner[11], M. Merk[41], D.A. Milanes[8], M.-N. Minard[4], J. Molina Rodriguez[60], S. Monteil[5], D. Moran[54], M. Morandin[22], P. Morawski[26], A. Mordà[6], M.J. Morello[23,s], J. Moron[27], R. Mountain[59], F. Muheim[50], K. Müller[40], R. Muresan[29], B. Muster[39], P. Naik[46], T. Nakada[39], R. Nandakumar[49], I. Nasteva[2], M. Needham[50], N. Neri[21], S. Neubert[38], N. Neufeld[38], M. Neuner[11], A.D. Nguyen[39], T.D. Nguyen[39], C. Nguyen-Mau[39,p], M. Nicol[7], V. Niess[5], R. Niet[9], N. Nikitin[32], T. Nikodem[11], A. Novoselov[35], A. Oblakowska-Mucha[27], V. Obraztsov[35], S. Oggero[41], S. Ogilvy[51], O. Okhrimenko[44], R. Oldeman[15,e], G. Onderwater[65], M. Orlandea[29], J.M. Otalora Goicochea[2], P. Owen[53], A. Oyanguren[64], B.K. Pal[59], A. Palano[13,c], F. Palombo[21,t], M. Palutan[18], J. Panman[38], A. Papanestis[49,38], M. Pappagallo[51], C. Parkes[54], C.J. Parkinson[9], G. Passaleva[17], G.D. Patel[52], M. Patel[53], C. Patrignani[19,j], A. Pazos Alvarez[37], A. Pearce[54], A. Pellegrino[41], M. Pepe Altarelli[38], S. Perazzini[14,d], E. Perez Trigo[37], P. Perret[5], M. Perrin-Terrin[6], L. Pescatore[45], E. Pesen[66], K. Petridis[53], A. Petrolini[19,j], E. Picatoste Olloqui[36], B. Pietrzyk[4], T. Pilař[48], D. Pinci[25], A. Pistone[19], S. Playfer[50], M. Plo Casasus[37], F. Polci[8], A. Poluektov[48,34], E. Polycarpo[2], A. Popov[35], D. Popov[10], B. Popovici[29], C. Potterat[2], A. Powell[55], J. Prisciandaro[39], A. Pritchard[52], C. Prouve[46], V. Pugatch[44], A. Puig Navarro[39], G. Punzi[23,r], W. Qian[4], B. Rachwal[26], J.H. Rademacker[46], B. Rakotomiaramanana[39], M. Rama[18], M.S. Rangel[2], I. Raniuk[43], N. Rauschmayr[38], G. Raven[42], S. Reichert[54], M.M. Reid[48], A.C. dos Reis[1], S. Ricciardi[49], A. Richards[53], K. Rinnert[52], V. Rives Molina[36], D.A. Roa Romero[5], P. Robbe[7], A.B. Rodrigues[1], E. Rodrigues[54], P. Rodriguez Perez[54], S. Roiser[38], V. Romanovsky[35], A. Romero Vidal[37], M. Rotondo[22], J. Rouvinet[39], T. Ruf[38], F. Ruffini[23], H. Ruiz[36], P. Ruiz Valls[64], G. Sabatino[25,l], J.J. Saborido Silva[37], N. Sagidova[30], P. Sail[51], B. Saitta[15,e], V. Salustino Guimaraes[2], C. Sanchez Mayordomo[64], B. Sanmartin Sedes[37], R. Santacesaria[25], C. Santamarina Rios[37], E. Santovetti[24,l], M. Sapunov[6], A. Sarti[18,m], C. Satriano[25,n], A. Satta[24], M. Savrie[16,f], D. Savrina[31,32], M. Schiller[42], H. Schindler[38], M. Schlupp[9], M. Schmelling[10], B. Schmidt[38], O. Schneider[39], A. Schopper[38], M.-H. Schune[7], R. Schwemmer[38], B. Sciascia[18], A. Sciubba[25], M. Seco[37], A. Semennikov[31], K. Senderowska[27], I. Sepp[53], N. Serra[40], J. Serrano[6], L. Sestini[22], P. Seyfert[11], M. Shapkin[35], I. Shapoval[16,43,f], Y. Shcheglov[30], T. Shears[52], L. Shekhtman[34], V. Shevchenko[63], A. Shires[9], R. Silva Coutinho[48], G. Simi[22], M. Sirendi[47], N. Skidmore[46], T. Skwarnicki[59], N.A. Smith[52], E. Smith[55,49], E. Smith[53], J. Smith[47], M. Smith[54], H. Snoek[41], M.D. Sokoloff[57], F.J.P. Soler[51], F. Soomro[39], D. Souza[46],

B. Souza De Paula[2], B. Spaan[9], A. Sparkes[50], F. Spinella[23], P. Spradlin[51], F. Stagni[38], S. Stahl[11],
O. Steinkamp[40], O. Stenyakin[35], S. Stevenson[55], S. Stoica[29], S. Stone[59], B. Storaci[40],
S. Stracka[23,38], M. Straticiuc[29], U. Straumann[40], R. Stroili[22], V.K. Subbiah[38], L. Sun[57],
W. Sutcliffe[53], K. Swientek[27], S. Swientek[9], V. Syropoulos[42], M. Szczekowski[28], P. Szczypka[39,38],
D. Szilard[2], T. Szumlak[27], S. T'Jampens[4], M. Teklishyn[7], G. Tellarini[16,f], E. Teodorescu[29],
F. Teubert[38], C. Thomas[55], E. Thomas[38], J. van Tilburg[41], V. Tisserand[4], M. Tobin[39], S. Tolk[42],
L. Tomassetti[16,f], D. Tonelli[38], S. Topp-Joergensen[55], N. Torr[55], E. Tournefier[4], S. Tourneur[39],
M.T. Tran[39], M. Tresch[40], A. Tsaregorodtsev[6], P. Tsopelas[41], N. Tuning[41], M. Ubeda Garcia[38],
A. Ukleja[28], A. Ustyuzhanin[63], U. Uwer[11], V. Vagnoni[14], G. Valenti[14], A. Vallier[7],
R. Vazquez Gomez[18], P. Vazquez Regueiro[37], C. Vázquez Sierra[37], S. Vecchi[16], J.J. Velthuis[46],
M. Veltri[17,h], G. Veneziano[39], M. Vesterinen[11], B. Viaud[7], D. Vieira[2], M. Vieites Diaz[37],
X. Vilasis-Cardona[36,o], A. Vollhardt[40], D. Volyanskyy[10], D. Voong[46], A. Vorobyev[30],
V. Vorobyev[34], C. Voß[62], H. Voss[10], J.A. de Vries[41], R. Waldi[62], C. Wallace[48], R. Wallace[12],
J. Walsh[23], S. Wandernoth[11], J. Wang[59], D.R. Ward[47], N.K. Watson[45], A.D. Webber[54],
D. Websdale[53], M. Whitehead[48], J. Wicht[38], D. Wiedner[11], G. Wilkinson[55], M.P. Williams[45],
M. Williams[56], F.F. Wilson[49], J. Wimberley[58], J. Wishahi[9], W. Wislicki[28], M. Witek[26],
G. Wormser[7], S.A. Wotton[47], S. Wright[47], S. Wu[3], K. Wyllie[38], Y. Xie[61], Z. Xing[59], Z. Xu[39],
Z. Yang[3], X. Yuan[3], O. Yushchenko[35], M. Zangoli[14], M. Zavertyaev[10,b], F. Zhang[3], L. Zhang[59],
W.C. Zhang[12], Y. Zhang[3], A. Zhelezov[11], A. Zhokhov[31], L. Zhong[3] and A. Zvyagin[38]

1   Centro Brasileiro de Pesquisas Físicas (CBPF), Rio de Janeiro, Brazil
2   Universidade Federal do Rio de Janeiro (UFRJ), Rio de Janeiro, Brazil
3   Center for High Energy Physics, Tsinghua University, Beijing, China
4   LAPP, Université de Savoie, CNRS/IN2P3, Annecy-Le-Vieux, France
5   Clermont Université, Université Blaise Pascal, CNRS/IN2P3, LPC, Clermont-Ferrand, France
6   CPPM, Aix-Marseille Université, CNRS/IN2P3, Marseille, France
7   LAL, Université Paris-Sud, CNRS/IN2P3, Orsay, France
8   LPNHE, Université Pierre et Marie Curie, Université Paris Diderot, CNRS/IN2P3, Paris, France
9   Fakultät Physik, Technische Universität Dortmund, Dortmund, Germany
10 Max-Planck-Institut für Kernphysik (MPIK), Heidelberg, Germany
11 Physikalisches Institut, Ruprecht-Karls-Universität Heidelberg, Heidelberg, Germany
12 School of Physics, University College Dublin, Dublin, Ireland
13 Sezione INFN di Bari, Bari, Italy
14 Sezione INFN di Bologna, Bologna, Italy
15 Sezione INFN di Cagliari, Cagliari, Italy
16 Sezione INFN di Ferrara, Ferrara, Italy
17 Sezione INFN di Firenze, Firenze, Italy
18 Laboratori Nazionali dell'INFN di Frascati, Frascati, Italy
19 Sezione INFN di Genova, Genova, Italy
20 Sezione INFN di Milano Bicocca, Milano, Italy
21 Sezione INFN di Milano, Milano, Italy
22 Sezione INFN di Padova, Padova, Italy
23 Sezione INFN di Pisa, Pisa, Italy
24 Sezione INFN di Roma Tor Vergata, Roma, Italy
25 Sezione INFN di Roma La Sapienza, Roma, Italy
26 Henryk Niewodniczanski Institute of Nuclear Physics Polish Academy of Sciences, Kraków, Poland
27 AGH - University of Science and Technology, Faculty of Physics and Applied Computer Science,
    Kraków, Poland
28 National Center for Nuclear Research (NCBJ), Warsaw, Poland
29 Horia Hulubei National Institute of Physics and Nuclear Engineering, Bucharest-Magurele,
    Romania

^{30} Petersburg Nuclear Physics Institute (PNPI), Gatchina, Russia

^{31} Institute of Theoretical and Experimental Physics (ITEP), Moscow, Russia

^{32} Institute of Nuclear Physics, Moscow State University (SINP MSU), Moscow, Russia

^{33} Institute for Nuclear Research of the Russian Academy of Sciences (INR RAN), Moscow, Russia

^{34} Budker Institute of Nuclear Physics (SB RAS) and Novosibirsk State University, Novosibirsk, Russia

^{35} Institute for High Energy Physics (IHEP), Protvino, Russia

^{36} Universitat de Barcelona, Barcelona, Spain

^{37} Universidad de Santiago de Compostela, Santiago de Compostela, Spain

^{38} European Organization for Nuclear Research (CERN), Geneva, Switzerland

^{39} Ecole Polytechnique Fédérale de Lausanne (EPFL), Lausanne, Switzerland

^{40} Physik-Institut, Universität Zürich, Zürich, Switzerland

^{41} Nikhef National Institute for Subatomic Physics, Amsterdam, The Netherlands

^{42} Nikhef National Institute for Subatomic Physics and VU University Amsterdam, Amsterdam, The Netherlands

^{43} NSC Kharkiv Institute of Physics and Technology (NSC KIPT), Kharkiv, Ukraine

^{44} Institute for Nuclear Research of the National Academy of Sciences (KINR), Kyiv, Ukraine

^{45} University of Birmingham, Birmingham, United Kingdom

^{46} H.H. Wills Physics Laboratory, University of Bristol, Bristol, United Kingdom

^{47} Cavendish Laboratory, University of Cambridge, Cambridge, United Kingdom

^{48} Department of Physics, University of Warwick, Coventry, United Kingdom

^{49} STFC Rutherford Appleton Laboratory, Didcot, United Kingdom

^{50} School of Physics and Astronomy, University of Edinburgh, Edinburgh, United Kingdom

^{51} School of Physics and Astronomy, University of Glasgow, Glasgow, United Kingdom

^{52} Oliver Lodge Laboratory, University of Liverpool, Liverpool, United Kingdom

^{53} Imperial College London, London, United Kingdom

^{54} School of Physics and Astronomy, University of Manchester, Manchester, United Kingdom

^{55} Department of Physics, University of Oxford, Oxford, United Kingdom

^{56} Massachusetts Institute of Technology, Cambridge, MA, United States

^{57} University of Cincinnati, Cincinnati, OH, United States

^{58} University of Maryland, College Park, MD, United States

^{59} Syracuse University, Syracuse, NY, United States

^{60} Pontifícia Universidade Católica do Rio de Janeiro (PUC-Rio), Rio de Janeiro, Brazil, associated to ^{2}

^{61} Institute of Particle Physics, Central China Normal University, Wuhan, Hubei, China, associated to ^{3}

^{62} Institut für Physik, Universität Rostock, Rostock, Germany, associated to ^{11}

^{63} National Research Centre Kurchatov Institute, Moscow, Russia, associated to ^{31}

^{64} Instituto de Fisica Corpuscular (IFIC), Universitat de Valencia-CSIC, Valencia, Spain, associated to ^{36}

^{65} KVI - University of Groningen, Groningen, The Netherlands, associated to ^{41}

^{66} Celal Bayar University, Manisa, Turkey, associated to ^{38}

^{a} Universidade Federal do Triângulo Mineiro (UFTM), Uberaba-MG, Brazil

^{b} P.N. Lebedev Physical Institute, Russian Academy of Science (LPI RAS), Moscow, Russia

^{c} Università di Bari, Bari, Italy

^{d} Università di Bologna, Bologna, Italy

^{e} Università di Cagliari, Cagliari, Italy

^{f} Università di Ferrara, Ferrara, Italy

^{g} Università di Firenze, Firenze, Italy

^{h} Università di Urbino, Urbino, Italy

^{i} Università di Modena e Reggio Emilia, Modena, Italy

[j] Università di Genova, Genova, Italy

[k] Università di Milano Bicocca, Milano, Italy

[l] Università di Roma Tor Vergata, Roma, Italy

[m] Università di Roma La Sapienza, Roma, Italy

[n] Università della Basilicata, Potenza, Italy

[o] LIFAELS, La Salle, Universitat Ramon Llull, Barcelona, Spain

[p] Hanoi University of Science, Hanoi, Viet Nam

[q] Università di Padova, Padova, Italy

[r] Università di Pisa, Pisa, Italy

[s] Scuola Normale Superiore, Pisa, Italy

[t] Università degli Studi di Milano, Milano, Italy